Stratified Spatiotemporal Chaos in Anisotropic Reaction-Diffusion Systems

Markus Bär,[1,3,*] Aric Hagberg,[2,†] Ehud Meron,[3,‡] and Uwe Thiele[1,4,§]

[1]*Max-Planck-Institut für Physik Komplexer Systeme, Nöthnitzer Strasse 38, 01187 Dresden, Germany*
[2]*Theoretical Division and Center for Nonlinear Studies, Los Alamos National Laboratory, Los Alamos, New Mexico 87545*
[3]*The Jacob Blaustein Institute for Desert Research and the Physics Department, Ben-Gurion University,*
Sede Boker Campus 84990, Israel
[4]*Instituto Pluridisciplinar, Universidad Complutense Madrid, Paseo Juan XXIII 1, E-28040 Madrid, Spain*

Numerical simulations of two-dimensional pattern formation in an anisotropic bistable reaction-diffusion medium reveal a new dynamical state, stratified spatiotemporal chaos, characterized by strong correlations along one of the principal axes. Equations that describe the dependence of front motion on the angle illustrate the mechanism leading to stratified chaos.

Pattern formation in nonequilibrium systems has been extensively studied in isotropic, two-dimensional media [1]. Among the most prominent experimental examples are Rayleigh-Benard convection and the Belousov-Zhabotinsky reaction in the contexts of fluid dynamics and chemical reactions, respectively. Recently, there has also been considerable interest in systems with broken rotational symmetry, such as convection in liquid crystals [2] and chemical waves in catalytic surface reactions [3]. Experimental and theoretical studies of such anisotropic systems showed novel phenomena such as ordered arrays of topological defects [4], anisotropic phase turbulence [5], reaction-diffusion waves with sharp corners [6], and traveling wave fragments along a preferred orientation [7]. Anisotropy is also often present in pattern formation processes in biological media, e.g., in cardiac tissue [8].

In this Letter we present a new dynamical state that is possible only in anisotropic media-stratified spatiotemporal chaos. We demonstrate the phenomenon with numerical simulations of the bistable FitzHugh-Nagumo equations with anisotropic diffusion and characterize it by computing orientation dependent correlation functions. In addition, an equation for the dependence of front velocities on parameters, curvature, and the angular orientation is derived. The mechanism leading to stratified chaos is described in terms of these analytic results. It is tightly linked to the anisotropy of the system and differs from the mechanism leading to spiral chaos in isotropic bistable media [9–11]. The findings here are relevant to catalytic reactions on surfaces where anisotropy is naturally provided by crystal symmetry and in biological tissue where anisotropy comes from fiber orientation.

Many qualitative features of pattern formation in chemical and biological reaction-diffusion systems are well described by FitzHugh-Nagumo type models for bistable media [12,13]. The specific model we choose to study is

$$\frac{\partial u}{\partial t} = \epsilon^{-1}(u - u^3 - v) + \delta^{-1}\nabla^2 u + \frac{\partial}{\partial y}\left[d\delta^{-1}\frac{\partial u}{\partial y}\right],$$

$$\frac{\partial v}{\partial t} = u - a_1 v - a_0 + \nabla^2 v, \tag{1}$$

where u is the activator and v the inhibitor. The parameters a_1 and a_0 are chosen so that Eqs. (1) represent a bistable medium with two stationary and uniform stable states, an "up" state, (u_+, v_+), and a "down" state, (u_-, v_-). Front solutions connect the two states. The number of front solutions changes, when a single front (an "Ising" front) that exists for values of $\eta := \sqrt{\epsilon\delta} > \eta_c$ loses stability to a pair of counterpropagating fronts ("Bloch" fronts) for $\eta \leq \eta_c$. The corresponding bifurcation is referred to as the nonequilibrium Ising-Bloch bifurcation, hereafter the "front bifurcation." The anisotropy of the medium is reflected through the parameter d.

Figure 1 shows the formation and time evolution of stratified chaos obtained by numerical solution of Eqs. (1). The initial state is isotropic spiral chaos. As time evolves a clear orientation of up-state (grey) domains along the y direction develops. The domains consist primarily of elongating stripe segments which either merge with other segments or shorten by emitting traveling blobs. The stratified chaos state is robust and develops from a variety of initial conditions including a single spot.

To gain insight we have followed the dynamics of u and v along the x and y axes and display them in the form of space-time plots in Fig. 2. A nearly periodic nonpropagating pattern along the x axis and irregular traveling wave phenomena along the y axis are observed. A characteristic property of spatiotemporal chaotic patterns is correlations that decay on a length scale ξ much smaller than the system length L. We have computed the normalized spatial two-point correlation functions, $C_y(r)$ and $C_x(r)$, for the u field in both the x and y directions, where $C_y(r) = \langle \Delta u(x, y + r)\Delta u(x,y)\rangle/\langle\Delta u(x,y)^2\rangle$, $C_x(r) = \langle \Delta u(x + r, y)\Delta u(x,y)\rangle/\langle\Delta u(x,y)^2\rangle$, $\Delta u(x,y) = u(x,y) - \langle u\rangle$, and the brackets $\langle\rangle$ denote space and time averaging. Figure 3
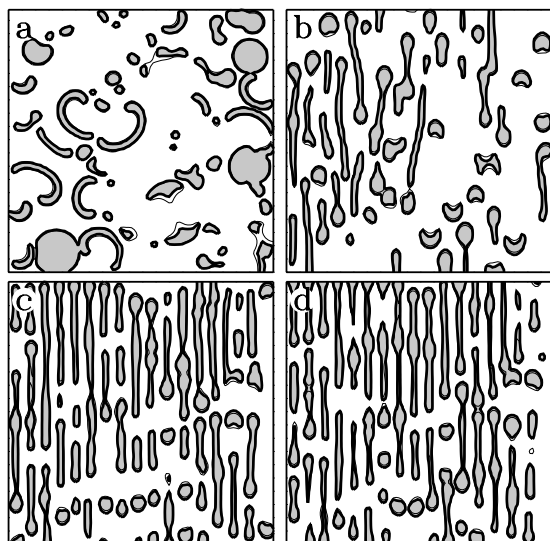
FIG. 1. The development of stratified spatiotemporal chaos from an initial state of isotropic spatiotemporal chaos. The thick contour line represents $u = 0$ and the thin contour line $v = 0$. The shaded regions are up-state domains. Parameters: $a1 = 2.0$, $a_0 = -0.1$, $\epsilon = 0.039$, $\delta = 1.7$, $d = 1.0$, $x = [0, 80]$, $y = [0, 80]$.

shows the results of these computations. Correlations in the y direction decay fast to zero, whereas correlations in the x direction oscillate with constant amplitude. This observation may be used to define stratified chaos as a
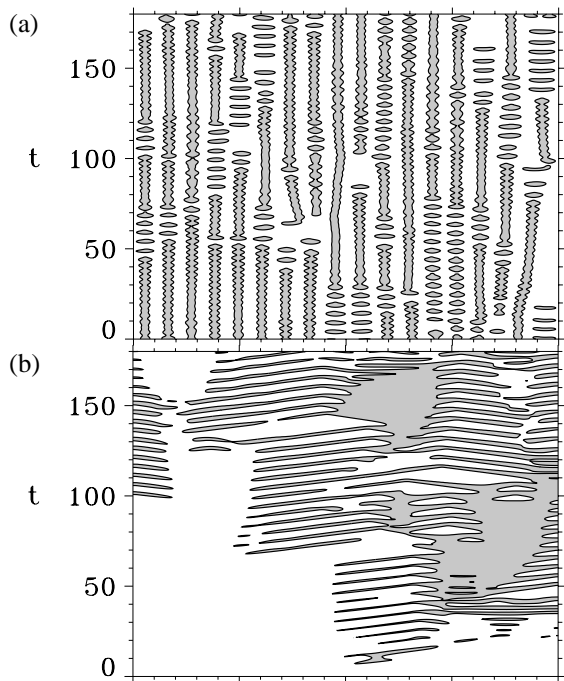

FIG. 2. Space-time plots of cuts parallel to the x axis (top) and the y axis (bottom) for the simulation of Fig. 1. The nearly vertical columns on the top figure show instances of periodic breathing motion of stripe segments (modulated continuous segments) and periodic blob formation (spot arrays).

state that displays finite correlation length in one direction (x) and infinite correlation length in the other (y).

An important analytical tool for studying front dynamics consists of relations between the normal front velocity C_n and other front properties like curvature. Relations of that kind have successfully been used in the study of pattern formation in isotropic media [10], and we exploit this tool for anisotropic media as well.

Velocity-curvature relations are derived here for $\lambda := \sqrt{\epsilon/\delta} \ll 1$. The first step in this derivation is to define an orthogonal coordinate system (r, s) that moves with the front, where r is a coordinate normal to the front and s is the arclength. We denote the position vector of the front by $\mathbf{X}(s, t) = (X, Y)$ and define it to coincide with the $u = 0$ contour line. The unit vectors tangent and normal to the front are given by $\hat{s} = \cos\theta\hat{x} + \sin\theta\hat{y}$ and $\hat{r} = -\sin\theta\hat{x} + \cos\theta\hat{y}$, respectively, where $\theta(s, t)$ is the angle that $\hat{s}$ makes with the x axis. A point $\mathbf{x} = (x, y)$ in the laboratory frame can be expressed as $\mathbf{x} = \mathbf{X}(s, t) + r\hat{r}$. This gives the following relations between the laboratory coordinates (x, y) and the coordinates (s, r) in the moving frame: $x = X(s, t) - r\sin\theta(s, t)$, and $y = Y(s, t) + r\cos\theta(s, t)$ where we defined $\hat{s} = \partial\mathbf{X}/\partial s$ and $\partial X/\partial s = \cos\theta$, $\partial Y/\partial s = \sin\theta$. In terms of the moving frame coordinates the front normal velocity and curvature are given by $C_n = -\frac{\partial r}{\partial t}$ and $\kappa = -\frac{\partial\theta}{\partial s}$, respectively.

The second step is to express Eqs. (1) in the moving frame and use singular perturbation theory, exploiting the smallness of λ. We distinguish between an inner region that includes the narrow front structure, and outer regions on both sides of the front. In the inner region $\partial u/\partial r \sim \mathcal{O}(\lambda^{-1})$ and $\partial v/\partial r \sim \mathcal{O}(1)$. In the outer regions both $\partial u/\partial r$ and $\partial v/\partial r$ are of order unity. In the inner region $v = v_f$ is taken to be constant. Expanding both u and v_f as powers series in λ and using these expansions in the moving frame equations we obtain, at order $\mathcal{O}(\lambda)$, a solvability condition that leads to the equation

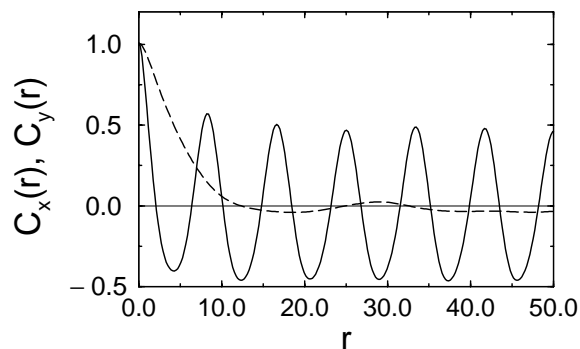$$C_n = -\frac{3}{\eta\sqrt{2}}I(\theta)v_f - \frac{1 + d}{\delta I(\theta)^2}\kappa, \qquad (2)$$

FIG. 3. Correlation functions $C_x(r)$ (solid curve) and $C_y(r)$ (dashed curve).

where $I(\theta) = \sqrt{1 + d\cos^2\theta}$. In the outer regions to the left and to the right of the front region different approximations can be made. Here $\frac{\partial u}{\partial r} \sim \frac{\partial v}{\partial r} \sim \mathcal{O}(1)$ and to leading order all terms that contain the factor λ can be neglected. The resulting equations can be solved for v in the two outer regions. Continuity of v and of $\frac{\partial v}{\partial r}$ at the front position $r = 0$ yields a second relation between C_n and v_f. Eliminating v_f by inserting this relation into Eq. (2) gives an implicit relation between the normal velocity of the front and its curvature

$$C_n + \frac{1+d}{\delta I(\theta)^2}\kappa = \frac{3I(\theta)(C_n + \kappa)}{\eta\sqrt{2}\,q^2\sqrt{(C_n + \kappa)^2 + 4q^2}} + \frac{3I(\theta)a_0}{\eta\sqrt{2}\,q^2},$$
$$(3)$$

where $q^2 = a_1 + 1/2$. A complete account of this derivation will be published elsewhere.

Figure 4 displays solutions of Eq. (3) showing the dependence of the front velocity on front curvature and propagation direction for the parameter values of Fig. 1. In Fig. 4a C_n vs κ relations are shown for two orthogonal propagation directions. In the x direction, $\theta = \pi/2$ (dashed curve), there is only one planar front solution with negative velocity (a down state invading an up state), indicating an Ising regime. The negative slope of the C_n vs κ relation implies stability to transverse perturbations. In the y direction, $\theta = 0$ (solid curve), there are three planar front solutions indicating a Bloch regime. The positive-velocity front (up state invading down state) is unstable to transverse perturbations whereas the negative velocity front is stable. The middle branch corresponds to an unstable front.

Figure 4b shows the angular dependence of planar-front velocities. Counterpropagating (Bloch) fronts exist in a narrow sector around the y direction ($\theta = 0$). The other directions support only a single (Ising) front. The Ising front speed is smallest in the x direction ($\theta = \pi/2$) and increases as θ deviates from $\pi/2$.

The dynamics of fronts as displayed in Fig. 1 are affected by curvature, propagation direction, and front interactions. Equation (3) captures the effects of the first two factors but does not contain information about front interactions. The necessary information for our purpose can be summarized as follows.

The time evolution of a pair of fronts approaching one another is affected by the speed of noninteracting fronts and by the diffusion rate of the activator u [assuming an inhibitor diffusion constant equal to unity as in Eqs. (1)]. Consider a pair of fronts pertaining to up states invading a down state, propagating toward one another in an isotropic medium ($d = 0$). If the distance between the fronts decreases below a critical value, $\lambda_c \sim \mathcal{O}(\sqrt{\epsilon/\delta})$, the two fronts collapse, leaving a uniform up state. The accumulation of the inhibitor in the space enclosed by the fronts, however, slows their motion. If the (noninteracting) front speed is low enough, or if λ is small enough, there is enough time for the inhibitor to slow the fronts down to a complete stop before they reach the critical distance λ_c. In that case the subsequent evolution depends on the front type. A pair of Ising fronts may form either a stationary pulse or, closer to the front bifurcation, a breathing pulse. A pair of Bloch fronts reflect and propagate away from one another [13]. Thus, high front speed or fast activator diffusion (δ small and λ_c large) lead to collapse, whereas low front speed and slow activator diffusion lead to strong front repulsion. A similar argument holds for down-state invading up-state fronts.

Returning to anisotropic media we need to know how the two factors that affect front interactions, front speed and activator diffusion, depend on the direction of propagation. The angular dependence of the front speed is already given in Fig. 4b. The angular dependence of the activator diffusion can be deduced by inspecting Eqs. (1). It is $1/\delta$ in the x direction and $(1 + d)/\delta$ in the y direction. Since $d > 0$ the activator diffusion constant increases as the propagation direction changes from the x direction to the y direction.

We can discuss now the mechanism of stratified chaos. As Fig. 4a shows, the x direction represents a system that supports stationary or breathing planar stripe patterns.
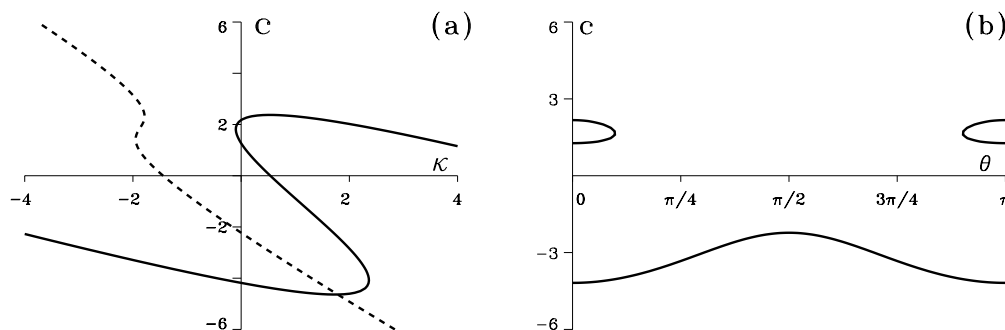

FIG. 4. Two views of the relation (3) corresponding to the parameters of the simulation in Fig. 1. (a) The velocity-curvature relation for fronts in the x direction (dashed curve) and y direction (solid curve). (b) The velocity of planar ($\kappa = 0$) fronts at different angles. Bloch fronts exist in narrow sectors around $\theta = 0$ and $\theta = \pi$. The wider sectors in between correspond to Ising fronts.
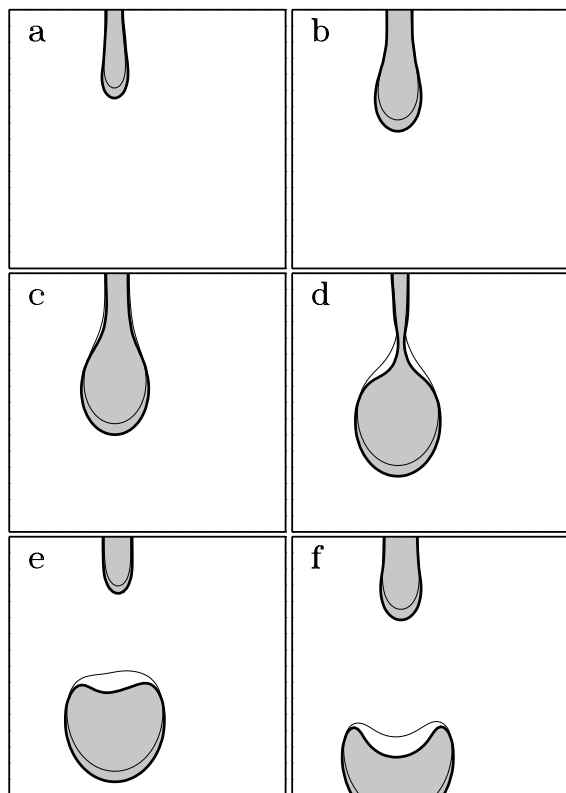
FIG. 5. Closeup of repeated blob formation. Shaded regions are up-state domains. Thick (thin) lines are $u = 0$ ($v = 0$) contours. The $v = 0$ line always lags behind the $u = 0$ line. The tip of a stripe segment (a) grows outward (b),(c). A pinching dynamics begins (d) which leads to blob formation (e) traveling along the y direction (f). The blob formation leaves a shortened stripe segment (e) whose tip grows outward again (f) and the process repeats. The parameters are the same as in Fig. 1.

The y direction represents a system where traveling waves prevail. The distinct characters of the medium along the two principal axes is reflected in the space-time plots of Fig. 2: nearly vertical columns in the x direction indicate stationary or breathing motion, and diagonal stripes in the y direction indicate traveling wave phenomena.

The irregular character of the dynamics comes from blob formation events as shown in Fig. 5. The front speed and activator diffusion in the x direction are sufficiently slow for Ising fronts to repel one another (rather than collapse). As the tip of the stripe segment grows outward and forms a bulge, propagation directions deviating from the x direction develop. At these directions both the front speed and the activator diffusion are higher. As a result approaching fronts may collapse. This is exactly the blob pinching process in frames (c), (d), and (e) of Fig. 5. The process is periodic for extended periods of time as indicated by the vertical spot arrays in Fig. 2.

In summary, stratified chaos relies on two main elements: (i) stationary or breathing domains vs traveling wave phenomena in orthogonal directions and (ii) an an-

gular dependence of front interactions that leads to blob formation. Without the second element stripe segments would merge to ever longer segments until a periodic stripe pattern is formed. These elements suggest the parameter regime where stratified chaos is expected to be found. The first element implies a regime along the front bifurcation such that there is stationary or breathing motion in the direction with faster activator diffusion and traveling waves in the other (slower diffusion) direction. The width of this regime increases with the anisotropy d. The second element implies that in the direction of breathing or stationary domains the system is close to the onset of breathing motion. Deviations from this direction which move the system toward the traveling wave regime then lead to front collapse. These expectations were verified numerically.

*baer@idefix.mpipks-dresden
†aric@lanl.gov
‡ehud@bgumail.bgu.ac.il
§thiele@nolineal.pluri.ucm.es

[1] M. C. Cross and P. C. Hohenberg, Rev. Mod. Phys. **65**, 851 (1993).

[2] L. Kramer and W. Pesch, Annu. Rev. Fluid. Mech. **27**, 515 (1995).

[3] R. Imbihl and G. Ertl, Chem. Rev. **95**, 697 (1995).

[4] M. Scheuring, L. Kramer, and J. Peinke, Phys. Rev. E **58**, 2018 (1998); G. D. Granzow and H. Riecke, Physica (Amsterdam) **249A**, 27 (1998).

[5] R. Faller and L. Kramer, Phys. Rev. E **57**, 6249 (1998).

[6] F. Mertens and R. Imbihl, Nature (London) **370**, 124 (1994); A. S. Mikhailov, Phys. Rev. E **49**, 5875 (1994); N. Gottschalk, F. Mertens, M. Bär, M. Eiswirth, and R. Imbihl, Phys. Rev. Lett. **73**, 3483 (1994).

[7] F. Mertens, N. Gottschalk, M. Bär, M. Eiswirth, A. Mikhailov, and R. Imbihl, Phys. Rev. E **51**, 5193 (1995).

[8] A. T. Winfree, Int. J. Bifurcation Chaos Appl. Sci. Eng. **7**, 784 (1997); J. Keener and J. Sneyd, *Mathematical Physiology* (Springer, New York, 1998).

[9] K. J. Lee and H. L. Swinney, Phys. Rev. E **51**, 1899 (1995); G. Li, Q. Ouyang, and H. L. Swinney, J. Chem. Phys. **105**, 10 830 (1996).

[10] A. Hagberg and E. Meron, Phys. Rev. Lett. **72**, 2494 (1994); Chaos **4**, 477 (1994).

[11] A. Hagberg and E. Meron, Phys. Rev. Lett. **78**, 1166 (1997); Physica (Amsterdam) **123D**, 460 (1998).

[12] H. Ikeda, M. Mimura, and Y. Nishiura, Nonlinear Anal. Theory Methods Appl. **13**, 507 (1989).

[13] A. Hagberg and E. Meron, Nonlinearity **7**, 805 (1994).